Carbohydrate Polymers 111 (2014) 813–821

Contents lists available at ScienceDirect

Carbohydrate Polymers

journal homepage: www.elsevier.com/locate/carbpol

Taguchi design and equilibrium modeling for fluoride adsorption on cerium loaded cellulose nanocomposite bead

Dhiman Santra, Rajib Joarder, Mitali Sarkar*

Department of Chemistry, University of Kalyani, Kalyani 741 235, India

ARTICLE INFO

Article history:
Received 21 November 2013
Received in revised form 11 May 2014
Accepted 13 May 2014
Available online 27 May 2014

Keywords:
Cerium loaded cellulose nanocomposite bead
Fluoride
Adsorption
Taguchi design tool
Isotherm
Regeneration

ABSTRACT

The cooperative influence of operational variables for fluoride adsorption on cerium loaded cellulose nanocomposite bead (CCNB) was assessed using Taguchi design tool. The percentage contribution of each operational variable was determined. The solution pH, with a maximum contribution of 80.78%, indicates its highest influence on the response, the adsorption percent of fluoride. The quality and validity of the experimental design were assessed from ANOVA and subsequently by the confirmation experiment. The equilibrium adsorption data showed that the Temkin isotherm is the most suited one compared to the Langmuir and Freundlich model. It is found that almost 90% adsorbed fluoride can be eluted with 0.01 (N) NaOH and the regenerated bead can successively be reused for at least three times.

1. Introduction

Fluoride in minute quantity, although, is an essential component for normal mineralization of bones and formation of dental enamel (Teutli-Sequeira, Solache-Ríos, & Balderas-Hernández, 2012), consumption of fluoride rich drinking water may cause fluorosis, a detrimental manifestation in human (WHO, 2008). Due to its high bioavailability fluoride may easily be absorbed by the gastrointestinal tract without intervention of interfering elements such as Ca^{+2}, Mg^{+2} and Al^{+3} (Viswanathan, Jaswanth, Gopalakrishnan, & Siva ilango, 2009). Fluoride reacts readily with the positively charged calcium and is known to affect predominantly the skeletal system, teeth, brain and spinal cord (Mohan, Ramanaiah, Rajkumar, & Sarma, 2007; Viswanathan & Meenakshi, 2008). Fluoride, even in a level of one part per million or less, is known to inhibit over 100 different enzyme systems, such as acetyl cholinesterase and ATPase which play important roles in brain and nerve function (Yiamouyiannis, 1983).

Conventional removal of fluoride following chemical precipitation (Chang & Liu, 2007), coagulation (Hu, Lo, & Kuan, 2005), lime treatment (Meenakshi & Maheshwari, 2006), ion exchange (Meenakshi & Viswanathan, 2007), membrane separation (Sehn, 2008) and electrolysis (Drouiche et al., 2008) have serious limitations in terms of high cost, techno feasibility, simplicity and generation of secondary pollutants. Jagtap, Yenkie, Labhsetwar, and Rayalu (2012) discussed the removal strategies together with the prevalence of fluoride in drinking water around the globe and the associated health menace. Adsorption is found to be a popular and cost effective simple approach considering its versatility for removal of a large variety of pollutants. Adsorptive removal from aqueous environment with the advantage of techno-feasibility and recycling of adsorbent using a range of adsorbents viz. activated carbon (Alagumuthu & Ranjan, 2010), alumina (Tang, Guan, Su, Gao, & Wang, 2009), sol–gel-derived activated alumina (Camacho, Torres, Saha, & Deng, 2010), calcite (Turner, Binning, & Stipp, 2005), fly ash (Sarkar, Manna, & Pramanik, 2008), bone char (Medellin-Castillo et al., 2007), laterite (Sarkar, Banerjee, Pramanik, & Sarkar, 2006) etc. are available. Improved fluoride adsorption was reported using different materials viz. resins, composites, oxides, gel, polymer, fibrous protein, carbon etc. modified with metals particularly aluminum (Luo & Inoue, 2004; Ramos, 1999), iron (Zhao, Li, Liu, & Chen, 2008), lanthanum (Fang, Ghimire, Kuriyama, Inoue, & Makino, 2003; Kamble et al., 2007; Rao & Karthikeyan, 2012; Wasay, Haron, & Tokunaga, 1996; Zhou, Yu, & Shan, 2004), cerium (Deng & Yu, 2012; Sivasankar, Murugesh, Rajkumar, & Darchen, 2013) and cerium-titanium (Xiuru, Kuanxiu, Jianping, Liuchang, & Zhaohui, 1998). Adsorbents derived from biomaterials such as chitin (Davila-Rodriguez, Escobar-Barrios,

* Corresponding author. Tel.: +91 033 2582 8750; fax: +91 033 2582 8282.
E-mail addresses: mitali_ku@yahoo.com, msarkar@klyuniv.ac.in (M. Sarkar).

http://dx.doi.org/10.1016/j.carbpol.2014.05.040
0144-8617/

Shirai, & Rangel-Mendez, 2009; Jayapriya, Ramya, Rathinam, & Sudha, 2011) and chitosan (Swain et al., 2010; Viswanathan, Sundaram, & Meenakshi, 2009) are particularly important in terms of their easy availability and biodegradable character. Cellulose being the most abundant natural polysaccharide might be a suitable renewable substrate material for the synthesis of adsorbent through modification with metal such as iron, aluminum, titanium, lanthanum, cerium etc. for fluoride removal.

The present study deals with modeling of fluoride adsorption using cerium loaded cellulose nanocomposite bead (CCNB) characterized by Fourier transform infrared spectroscopy (FTIR), field emission scanning electron microscopy (FESEM), energy dispersive spectroscopy (EDS) and electron paramagnetic resonance (EPR) study. In an aim to improve the precision of operation simultaneous optimization of process variables was made using statistical design of experiment following Taguchi tool. Taguchi tool utilizes a standard orthogonal array comprising of each experimental variable with different levels. The signal-to-noise (S/N) ratio corresponding to each combination is computed and is analyzed, based on ANOVA, to determine the optimal settings (experimental variable with its level) as well as the validity of the design. The feasibility of adsorption was determined following isotherm analysis. The utility of the present adsorbent was judged from the regeneration study.

2. Experimental

2.1. Materials

All the chemicals and solvents used are of analytical grade (Merck, India). The cellulose power used was procured from Loba Chemie, Mumbai, India.

2.2. Preparation of CCNB

Cerium loaded cellulose nanocomposite bead was synthesized by wet chemical process via sol–gel formation technique (Hench & West, 1990). 1.0 g of cellulose powder (precursor) was first soaked in 20 mL of 19% (w/w) aqueous sodium hydroxide (NaOH) which on aging for 3 days at room temperature yields a colloidal suspensions, the sol. 1.0 mL of carbon disulfide was subsequently added to the mixture and shaken (150 spm) for 8 h for esterification. 10 ml of 6% (w/w) NaOH solution was added to the sol of esterified cellulose and stirred for 3 h (Wang, Hao, Shi, & Sun, 2007) and allowed for syneresis at room temperature for 72 h. The viscose solution, the gel formed by condensation of the sol, was purged drop by drop into de-aerated methanol through a needle. Faintly red colored beads initially formed were filtered and immediately washed several times with double distilled water. The cellulose beads appeared as snow white, were stored under de-ionized water. It is probable that the sol–gel transition controls the shape and size of the formed cellulose nanocomposite bead.

The cellulose beads were next poured into a solution of 0.10 M cerium ammonium nitrate at pH 1.6 and shaken at a speed of 100 spm at room temperature for 2 h. A faint orange yellow colored cerium loaded cellulose nanocomposite bead, (CCNB) was formed, washed with distilled water and stored under de-ionized water.

2.3. Characterization of CCNB

CCNB was characterized by field emission scanning electron microscope (FESEM) with a JEOL, JSM 6700F microscope to study its surface morphology and energy dispersive spectroscopy (EDS) with FEI QUANTA FEG 250 for element detection. Electron paramagnetic resonance (EPR) spectrum, to identify the binding pattern of cerium in the bead, was recorded with a Varian X-band EPR spectrometer (Model E-109). The Fourier transformed infrared (FTIR) spectral study was carried out using Perkin Elmer L120-000A.

2.4. Batch adsorption and regeneration studies

Batch adsorption experiment was performed for fluoride adsorption on CCNB in a 100 mL Teflon stoppered conical flask. 25 mL of fluoride solution at a concentration of 2.0–10 mg L^{-1} was shaken with 1.0 g of CCNB for 1 h at a constant shaking rate of 120 spm in a temperature-controlled shaker until the equilibrium is attained. The initial solution pH was adjusted using either 0.1 M HCl or 0.1 M NaOH. The experiment was performed at different temperatures ranging from 293 to 323 K. Fluoride concentration in solution was determined potentiometrically using fluoride ion sensitive electrode (9609BNWP) in an Orion ion meter (VSTAR52). Adsorption efficiency, expressed as percent adsorption, was calculated using the following equation:

$$\text{percent adsorption}\,(\%) = \frac{(C_0 - C_e)\cdot 100}{C_0} \quad (1)$$

where C_0 and C_e are the initial and equilibrium fluoride concentration (mg L^{-1}) respectively in solution.

The elution of fluoride and regeneration of CCNB were made using definite concentration of NaOH in batch mode.

2.5. Statistical design of experiment using Taguchi tool

The design of adsorption experiment through Taguchi tool was made with the following objectives:

(i) to select the appropriate orthogonal array (OA) using each operational variable with all selected levels,
(ii) to categorize the variables and analyze the design quality from statistical analysis of variance (ANOVA),
(iii) to predict the response (percent adsorption) at the optimum level of the operational variables,
(iv) to run a confirmation experiment for validation of the predicted response.

2.5.1. Selection of orthogonal array (OA) and statistical analysis

An orthogonal array is made using five operational variables [pH, concentration (mg L^{-1}), adsorbent dose (g L^{-1}), contact time (min) and temperature (°C)] each with four levels and combinations in equal number of occurrence (Table 1) to yield a balanced design.

Taguchi approach based on the analysis of loss function was applied to yield the signal-to-noise (S/N) ratio and is used as the guiding parameter to judge the quality of experiment together with the validity of the result (response) (Atil & Unver, 2000). The S/N ratio, in fact, reflects the variability or level of precision of each response for each single experiment (trial) in the total set (replication). Any factor affecting the precision, mostly random and inherent for the operation, is termed as the noise. The response corresponding to the change of each operational variable is known as the signal which is used to correlate the response with the value of the operational variable.

Usually, three categories of S/N ratio analysis viz. 'larger is better' (LIB), 'nominal is best' (NIB) and 'smaller is better' (SIB) are available (Box, 1988; Ross, 1995). As the present study demands maximum adsorption, S/N ratio analysis following Eq. (2) for the LIB category is applied.

$$\frac{S}{N} = -10\log\frac{1}{n}\left(\sum\frac{1}{y^2}\right) \quad (2)$$

where n is the number of observations, and y is the observed response (adsorption percent).

Table 1
Orthogonal array of the operational variables each at four different levels.

Sl. no.	Level					Percent adsorption (%)			S/N ratio (dB)
	A	B	C	D	E	1st run	2nd run	Average	
1	1.5	2.5	0.3	20	20	76	79	77.5	37.7811
2	1.5	4	0.5	40	30	82	81	81.5	38.2226
3	1.5	5.5	0.7	60	40	82	82	82	38.2763
4	1.5	7	0.9	80	50	79	80	79.5	38.0068
5	3	2.5	0.5	60	50	89	85	87	38.7835
6	3	4	0.3	80	40	85	82	83.5	38.4295
7	3	5.5	0.9	20	30	80	78	79	37.9504
8	3	7	0.7	40	20	78	76	77	37.7276
9	4.5	2.5	0.7	80	30	75	75	75	37.5012
10	4.5	4	0.9	60	20	72	73	72.5	37.2061
11	4.5	5.5	0.3	40	50	70	71	70.5	36.9631
12	4.5	7	0.5	20	40	73	72	72.5	37.2061
13	6	2.5	0.9	40	40	70	73	71.5	37.0804
14	6	4	0.7	20	50	68	69	68.5	36.7131
15	6	5.5	0.5	80	20	63	63	63	35.9868
16	6	7	0.3	60	30	62	60	61	35.7031

The S/N ratio values thus obtained were analyzed for selection of the optimum condition (Seifi et al., 2011). At the optimum condition the statistical quality of the response was predicted from the analysis of variance (ANOVA) through sum of square, mean square, *F* ratio and *P* values (Soleimani & Kaghazchi, 2008; Zolfaghari et al., 2011). The prediction of response at the desired confidence level was made and validated with the experimental response through confirmation experiment (Ross, 1995; Srivastava, Mall, & Mishra, 2007). The layout of the orthogonal array [L_{16} (4^5)] considering five operational variables, viz.,. A: pH; B: concentration, C: adsorbent dose; D: contact time and E: temperature, each taken at four levels is shown in Table 1. Only sixteen experiments are needed to design the simultaneous influence of operational variables. Each experiment was repeated twice (1st run and 2nd run) and the S/N ratio was determined using Minitab software (version 15).

3. Results and discussion

3.1. Characterization of CCNB

3.1.1. FESEM and EDS analysis

The surface characteristic of the CCNB was investigated through FESEM and EDS analyses. The nanocomposite nature of the bead of average size in the range of 28–61 nm and spherical shape is revealed from the FESEM image. FESEM images of the bead at four different magnifications together with its physical look are presented in Fig. 1(a–e). Smaller particle size increases the effective surface area and available binding sites resulting efficient adsorption. EDS analysis shows peaks corresponding to 'C' and 'O' of cellulose as well as 'Ce' (Fig. 1f) in CCNB. The new peak around 0.7 keV appeared in the bead after fluoride adsorption (Fig. 1g) may be due to the one or both of 'F' and 'Ce'. High resolution of the spectrum of Fig. 1g was further taken in the region 0.10–1.00 keV (Fig. 1h). This clearly indicates two distinct peaks, corresponding to the K shell of 'F' and the M shell of 'Ce'. However, peak due to 'H' in cellulose does not appear in EDS.

3.1.2. EPR analysis

In order to identify the binding pattern of cerium in the bead EPR measurement was performed at 303 K and 77 K with the center magnetic field of 3300 G. The observed signals may attribute to the presence of Ce^{3+} sites in CCNB. The free Ce^{3+} ion has a $4f^1$ configuration, with $2S + 1L_J = 2F_{5/2}$ ground state, where S, L and J are the spin, orbital and total moments respectively. At 303 K the EPR exhibits mainly three signals at *g* values corresponding to 2.04, 1.94 and 1.89 G (Fig. 2a). At low temperature (77 K) similar spectrum characteristic with peaks at 2.03, 1.98 and 1.93 G was observed (Fig. 2b). The *g* values may be attributed to $g_e = 2.03$, $g_\perp = 1.98$, $g_{||} = 1.93$, characteristic of Ce^{3+} ($g_e > g_\perp > g_{||}$) (Abi-aad, Bechara, Grimblot, & Aboukais, 1993)]. There is a minor difference in the EPR signals in the spectrum at room temperature (303 K) and low temperature (77 K). A minor splitting of the broad signal at the *g* value 2.04 was observed at the lower temperature. The pattern and number of signals being practically the same, the restriction of movement of the Ce^{3+} ion in the bead may be indicated. This confirms that the Ce^{3+} moiety has been trapped inside some cage during the reaction. It is probable that Ce^{4+} in solution condition has converted to the Ce^{3+} and incorporated in the bead (Binnemans, 2006, Chap. 229).

3.1.3. FTIR analysis

The FTIR spectra of cellulose bead (CB) and CCNB respectively are shown in Fig. 2c and d, while Fig. 2e represents that after fluoride adsorption on CCNB. The broad band around 3402 cm^{-1} is attributed to the hydrogen bonding from —OH of cellulose. The band at 2918 cm^{-1} corresponds to the C—H stretching vibration and the band at 1642 cm^{-1} represents the molecular water bending mode, indicating the presence of physisorbed water of the beads. The characteristic absorption bands at 1424, 1375–1317, 1161, 1060 and 898 cm^{-1} are assigned to C—O—H and C—C—H deformations (1424 cm^{-1}), C—H flexure vibration (symmetric) (1375–1317 cm^{-1}), C—O stretching vibration (1161 cm^{-1}) C—O—H deformation (1060, 1035 cm^{-1}) and C—H bending vibration from the β-anomeric linkage (898 cm^{-1}) of cellulose. Modification of CB with cerium yields a new peak (Fig. 2d) at around 535 cm^{-1}, characteristic of metal-oxygen vibration, and is assigned for the presence of Ce—O linkage in CCNB (Li et al., 2010; Rocha & Muccillo, 2003). Consequently, increased band intensity at 1384 and 769 cm^{-1} is observed. Further, the bands at 1161 as well as 1060 and 1035 cm^{-1} in CB were found to somewhat decrease and a peak at 1120 cm^{-1} becomes prominent. The bands at 1120 and 1060 cm^{-1} are attributed to the bending mode of Ce—OH (Nakamoto, 1978); the band at 1060 cm^{-1} of CB, however, overlaps with that of Ce—OH after cerium loading (Li et al., 2010). Such changes after cerium loading may suggest the linkage of cerium via —C—O— groups of cellulose (Jagtap et al., 2009). This can further be supported by loading an excess amount of cerium to the cellulose bead. The band intensity at 1120 cm^{-1} becomes much prominent, however, that at 1060 cm^{-1} does not alter much. As this kind of bead very unstable fluoride adsorption experiment was carried out with cerium loaded cellulose bead maintaining optimum loading.

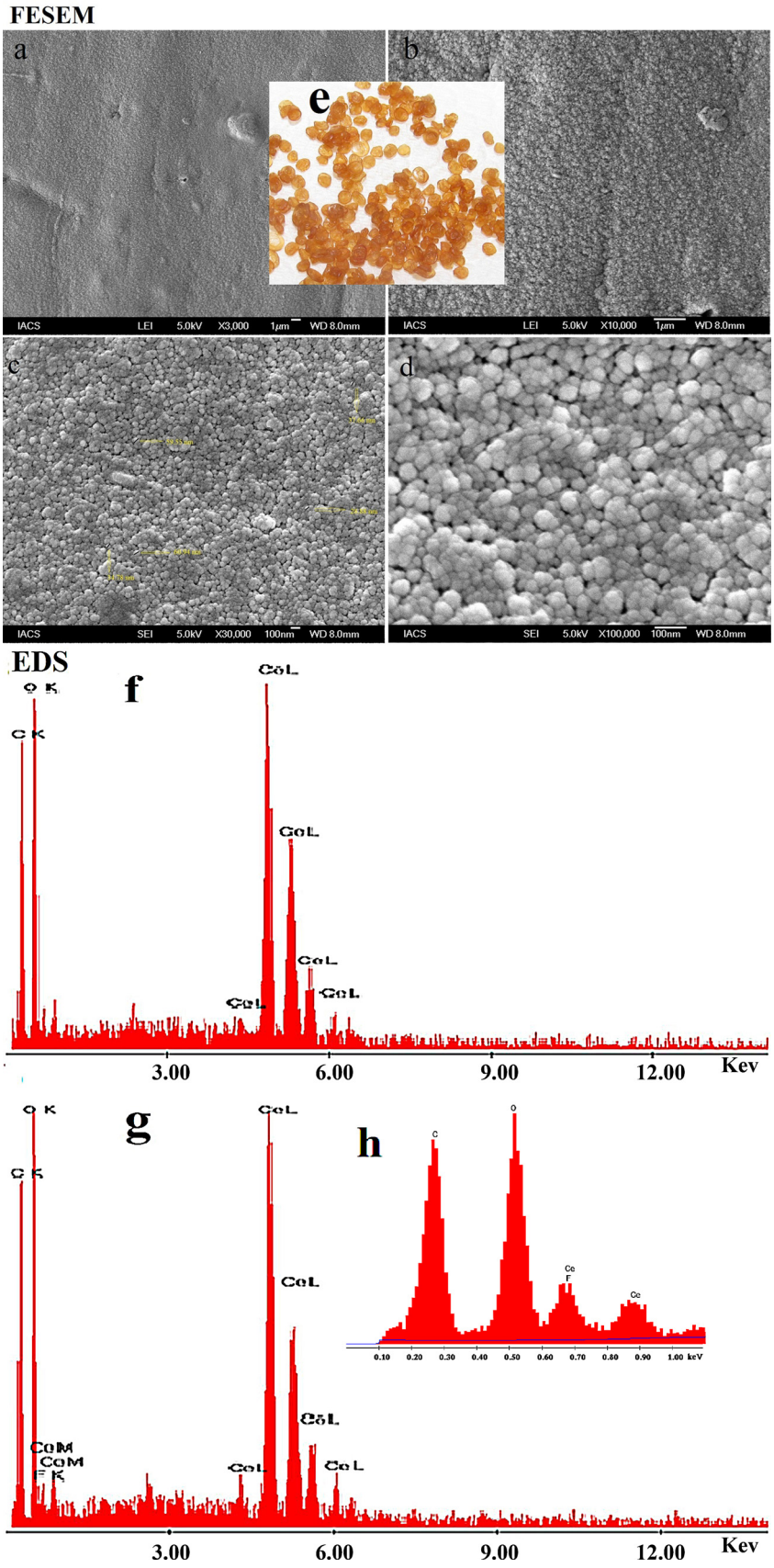

Fig. 1. FESEM of CCNB (a)–(e) at four different magnifications and the physical look. EDS of CCNB (f) before and (g) after adsorption (h) high resolution of (g).

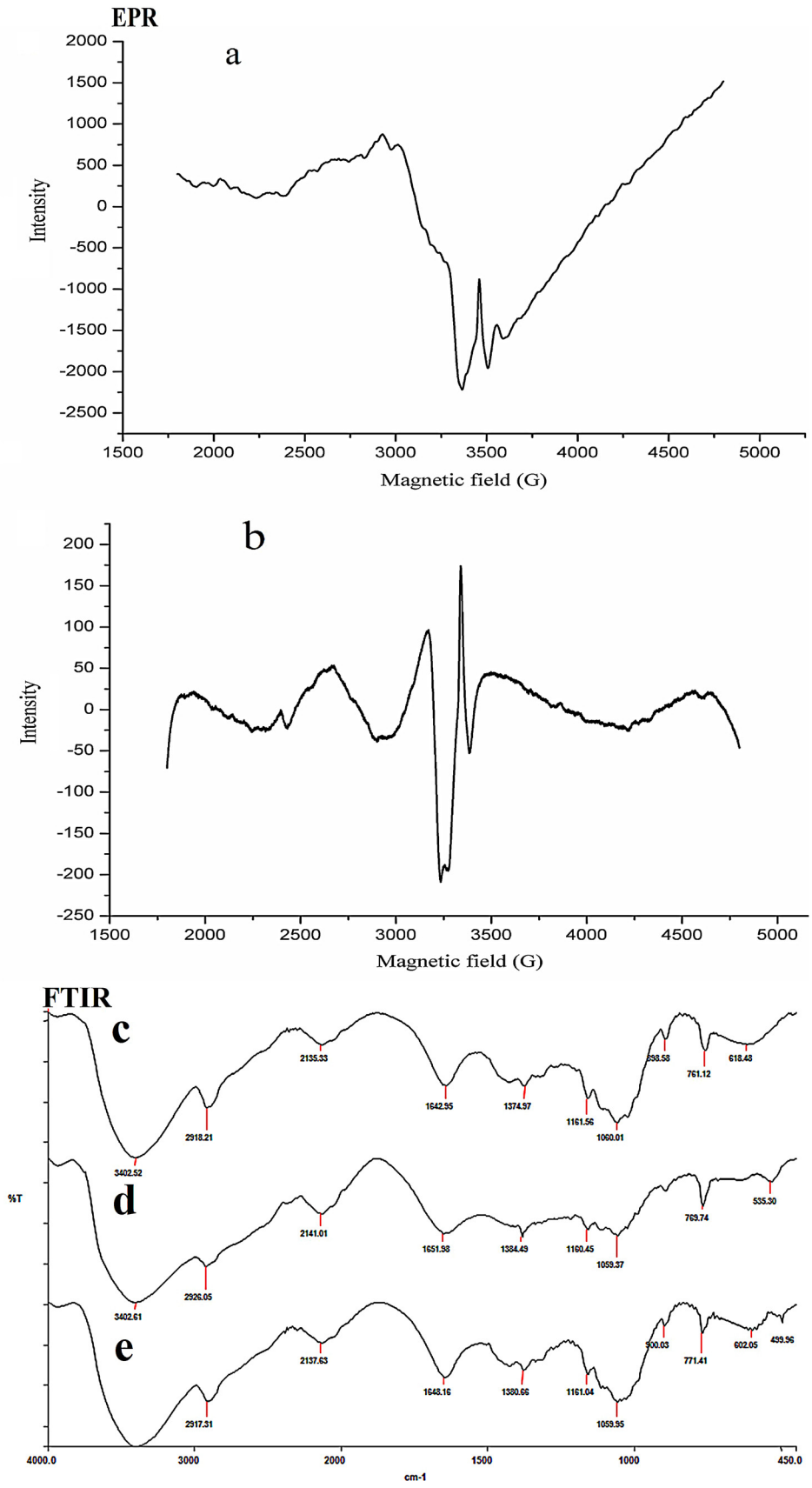

Fig. 2. EPR of CCNB at: (a) 303 K and (b) 77 K. FTIR of (c) cellulose bead, CCNB (d) before and (e) after adsorption.

Table 2
Characteristics mean S/N ratios following LIB category.

Level	A	B	C	D	E
1	38.07	37.79[a]	37.22	37.41	37.18
2	38.22[a]	37.64	37.55	37.50[a]	37.34
3	37.22	37.29	37.55	37.49	37.75[a]
4	36.37	37.16	37.56[a]	37.48	37.62
Δ	1.85	0.63	0.34	0.09	0.57
Rank	1	2	4	5	3

[a] The maximum mean S/N ratio indicative of optimum condition.

The FTIR spectrum of CCNB after fluoride adsorption clearly indicates that the band at 1120 cm^{-1} diminishes with changing band environment at 1060 cm^{-1}. A significant intensity change and shifting of the band position to 499 from 535 cm^{-1} (Fig. 2e) was, further, observed. This indicates some kind of interaction of fluoride with cerium. Since OH group and fluoride ion have similar dimension it is probable that they isomorphously replace each other through ligand exchange. This assumption was verified from the disappearance of band at 1120 cm^{-1} of CCNB when treated with higher concentration (10 mg L^{-1}) of fluoride. The shifting of the band from 535 to 499 cm^{-1} is attributed to the changes in the microenvironment of —C—O—Ce after replacement of OH by F (Sujana, Soma, Vasumathi, & Anand, 2009).

3.2. Taguchi design tool

3.2.1. OA and the analysis of S/N ratio

The value of the response (percent adsorption) as well as the S/N ratio corresponding to the [L_{16} (4^5)] orthogonal array, built for the present case, is determined (Table 1). The value of the mean S/N ratio was analyzed and the optimum level of operational variables is determined from the highest value. The influence of the operational variables on fluoride adsorption was known from the rank, as estimated from the max–min (Δ) value (Table 2). The optimum combination was found to be A2-B1-C4-D2-E3 with corresponding S/N ratio value 38.22, 37.79, 37.56, 37.5 and 37.75.

3.2.2. Statistical analysis of variance (ANOVA)

The percentage contribution of each operational variable to the response was determined in the primary analysis of variance (ANOVA) of the S/N ratio and is presented in Table 3. The order was found to be pH (80.78%) > concentration (9.34%) > temperature (3.08%) > adsorbent dose (3.082%) > contact time (0.002%) respectively. Considering the smallest and non-significant (0.002%) contribution, the operational variable *D*, was pooled into the error term.

The validity and significance of the design model were characterized from the model *F*-value, predicted *R*-squared value and adjusted *R*-squared value, using pooled ANOVA (Table 3). The model *F*-value of 145.75 implies the design model is significant. There is only a 0.08% chance that this large "Model *F*-Value" could occur due to noise. The predicted R-squared value (0.9513) found is in good agreement with the adjusted R-squared value (0.9914). *P*-value "Prob > *F*" less than 0.0500 indicates the variable is significant while that greater than 0.1000 indicates the variable is not significant.

Thus the variables A, B, C and E at the designated levels (2, 1, 4 and 3 respectively) are significant and hence the optimum combination is recommended to be A2-B1-C4-E3 for effective adsorption of fluoride on CCNB.

3.2.3. Performance prediction and confidence interval

With the optimum combination of operational variables (A2-B1-C4-E3), the theoretically predicted optimum S/N ratio η_{opt}, can be obtained (Srivastava et al., 2007) from the following equation:

$$\eta_{opt} = m_t + \sum_{i=1}^{n} (\eta_i - m_t) \quad (3)$$

where m_t and η_i are the overall mean and individual S/N ratio at the optimal level, n is the number of the operational variables. In the present case, the number of operational variables being 4, η_{opt} is calculated as:

$$\eta_{opt} = 37.47 + (38.22 - 37.47) + (37.79 - 37.47) + (37.56 - 37.47) + (37.75 - 37.47)$$

and is found to be 38.91.

The estimation of η_{opt} is only a point estimate based on the average value of results of the experiment. It is evident statistically, that chance of the true average being greater than η_{opt} is 50% with an equal chance being less than η_{opt}. Therefore, the confidence interval, C.I., which represents a range within which it is likely to fall the experimental value for a given level of confidence is estimated (Ross, 1995) following the expression (4):

$$\text{C.I.} = \pm\sqrt{\left[\frac{F_\alpha(1, f_e)V_e}{N_e}\right]} \quad (4)$$

where $F_\alpha(1, f_e)$ is the *F*-value at a confidence level of $(1-\alpha)$ against degree of freedom (df) 1, f_e is the df of error term and V_e is the error

Table 3
ANOVA of the S/N ratio for fluoride adsorption.

Mode	Operational variable	df	SS	MS	*F* value	*P*-value Prob > *F*	P.C (%)
Primary	A	3	8.799156	2.933052			80.078
	B	3	1.02615	0.34205			9.338
	C	3	0.33868	0.112893			3.082
	D	3	0.018816	0.006272			0.002
	E	3	0.805542	0.268514			7.330
	Error	0	0				
	Corr. total	15	10.98834				100
Pooled	A	3	8.7991	2.933052	467.646	0.0002[s]	79.90
	B	3	1.0261	0.34205	54.5364	0.0041[s]	9.17
	C	3	0.3387	0.112893	17.9997	0.0202[s]	2.91
	D	{3}		Pooled			
	E	3	0.8055	0.268514	42.8119	0.0058[s]	7.16
	Error	3	0.0188	0.006272			0.86
	Corr. total	15	10.9883				100

[s]: significant; SS: sum square; MS: mean square; P.C: percentage contribution.

variance or mean square error (from ANOVA). The mathematical parameter N_e can be expressed (Eq. (5)) as:

$$N_e = \frac{N}{1 + \mathrm{df_{opt}}} \tag{5}$$

where N is the total number of experimental run required as per the selected OA [L_{16} (4^5), in the present case] and $\mathrm{df_{opt}}$ represents the total degree of freedom of the operational variables (with its levels) used to estimate the value of η_{opt}. $F_{0.05}$ (1,3) [the F-value at the 95% confidence level and at the degree of freedom (df) of 1 and df of error (f_e) of 3] is obtained to be 10.13 from the above pooled ANOVA (Fischer, 1925). At the required number of experimental run (N = 16, as per OA), the pooled ANOVA (Table 3) estimates the value of V_e (=0.00627) and $\mathrm{df_{opt}}$ (=12). The confidence interval is, thus, calculated to be ±0.227, where N_e is 1.23077.

From the above calculation, the predicted S/N ratio is found to lie in the range 38.91 ± 0.227, i.e., between 38.68 and 39.14 dB. The predicted S/N ratio can be used to calculate the predicted response (y), the adsorption efficiency of the CCNB, for the LIB category using Eq. (2) as:

$$38.91 = -10 \log \frac{1}{n}\left(\sum \frac{1}{y^2}\right) = 20 \log y \tag{6}$$

and is found to be 88.21%, with the expected range between 85.90 and 90.57 at the estimated confidence interval.

3.2.4. Confirmation experiment

In order to test the validity of predicted response, experiments were carried out in three successive operations and the adsorption percent (response) of fluoride on CCNB were found to be 87.2, 89.0 and 90.1%. The corresponding S/N ratio was and found to be 38.78, 38.98 and 39.08 respectively using Eq. (2). The predicted value ranges of the percent adsorption and S/N ratio, based on the confidence interval, were calculated to be 85.90–90.57% and 38.68–39.14 dB respectively. As the mean adsorption percentage (88.66%) and the mean S/N ratio (38.94 dB) found to lie within the predicted value ranges the Taguchi design tool with selected optimum combination (A2-B1-C4-E3) is said to be valid.

3.3. Adsorption isotherm

In an aim to describe the equilibrium adsorption for fluoride ions from aqueous solution on CCNB Langmuir, Freundlich and Temkin isotherm were tested.

The Langmuir isotherm, applicable for the monolayer adsorption (Ho, Huang, & Huang, 2002) is expressed in its linear form as:

$$\frac{C_e}{q_e} = \left(\frac{1}{Q_b}\right) + \left(\frac{1}{Q}\right) C_e \tag{7}$$

where Q (mg g^{-1}) and b (L mg^{-1}) are Langmuir isotherm constants signifying the adsorption capacity and the energy of the adsorption respectively.

The Freundlich isotherm assuming an exponentially decaying adsorption site energy distribution and applicable to non-ideal adsorption on heterogeneous surfaces showing multi-layer adsorption (Al Duri & Mckay, 1988) is expressed by the following linear equation:

$$\ln q_e = \ln K_F + \left(\frac{1}{n_F}\right) \ln C_e \tag{8}$$

where K_F is the constant indicative of the relative adsorption capacity of the adsorbent (mg g^{-1}), and $1/n_F$ is the constant indicative of the intensity of the adsorption.

The Temkin isotherm (Allen, Mckay, & Porter, 2004) that considers solute/adsorbent interactions based on decaying heat of adsorption of the solute linearly with adsorbent surface coverage is represented in linear form as:

$$q_e = \left(\frac{RT}{b_{TM}}\right) \ln k_{TM} + \left(\frac{RT}{b_{TM}}\right) \ln C_e \tag{9}$$

where k_{TM} is the isotherm constant and b_{TM} is related to heat of adsorption.

The adsorption equilibrium data for fluoride adsorption at three different temperatures were fitted to the above three isotherm equations. In order to test the applicability of a particular isotherm model the experimentally determined equilibrium adsorption data was compared with that from calculated theoretically from each isotherm expression (Table 4).

Table 4
Isotherm parameters.

Isotherm	Temperature (K)	q_e (mg g^{-1})		R^2	SE
		expt	theo		
Langmuir	293	0.089	0.081	0.993	0.832
	303	0.094	0.081	0.975	1.531
	313	0.095	0.082	0.986	0.949
Freundlich	293	0.089	0.095	0.982	0.078
	303	0.094	0.104	0.954	0.127
	313	0.095	0.105	0.961	0.119
Temkin	293	0.089	0.084	0.995	0.007
	303	0.094	0.095	0.969	0.020
	313	0.095	0.095	0.985	0.015

The quality of data fit was judged from the R^2 and SE values. Higher R^2 and lower SE describe the most preferred situation. It is found that of the three different isotherm models R^2 values corresponding to Langmuir and Temkin are higher than the Freundlich model. The suitability of Langmuir or Temkin model is, therefore, assessed by comparing the SE values, which is found to be much lower for Temkin isotherm. Thus, Temkin isotherm model most suitably describes the fluoride adsorption on CCNB.

3.4. Elution of fluoride and reusability of CCNB

In practical applications the solute after adsorption needs to be eluted and adsorbent is reused/recycled. Elution of fluoride with 0.01 (N) NaOH was found effective and almost 95% of adsorbed fluoride can be eluted in a small volume of NaOH. The regenerated bead can be recycled for fluoride adsorption at least for three successive operations without compromising the adsorption capacity. However, use of NaOH in higher concentration (0.1 N) though retains higher adsorption percent (90%) subsequently decreases the adsorption extent to 32% after three successive cycles with the renewed adsorbent (Fig. 3) with simultaneous degradation of the bead. Thus elution of fluoride is recommended with 0.01 (N) NaOH.

3.5. Mechanism of fluoride adsorption on CCNB

Adsorption is a complex phenomenon involving both specific and non-specific interactions between the solute and the adsorbent. In CCNB presence of Ce is evidenced from EDS and binding with cellulose moiety via —O-linkage from FTIR. The disappearance of band at 1120 cm^{-1} as well as significant shifting and intensity change of the peak from 535 cm^{-1} to 499 cm^{-1} (Fig. 2e) in FTIR and appearance of peak due to F in EDS (Fig. 1g and h) further supports some kind of cerium —F interaction during adsorption. It is found that the solution pH plays an important role governing fluoride adsorption on CCNB. As the pH increases the adsorption was found to increase up to a pH value of 3.0 and subsequently falls beyond pH 3.0 (Fig. 4).

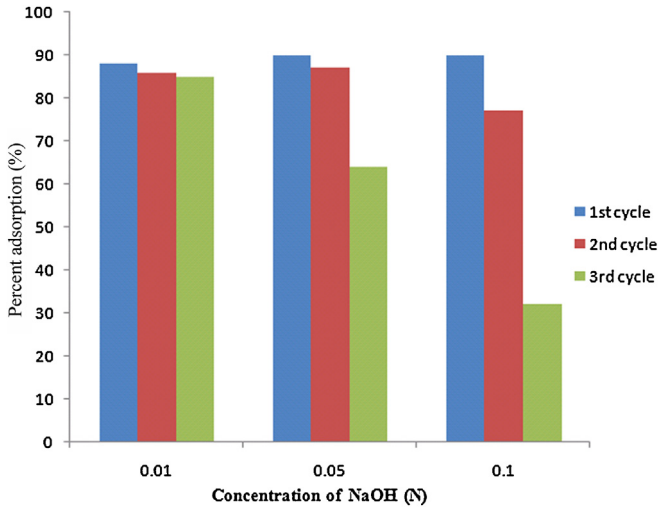

Fig. 3. Regeneration and recycling of CCNB.

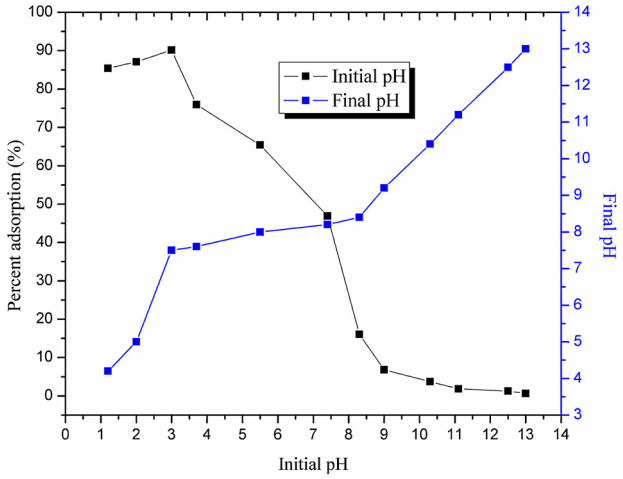

Fig. 4. pH dependent adsorption behavior of fluoride on CCNB.

At the acidic pH the CCNB-F interaction may be explained by the following pathways (i)–(iii). The pathways (i) and (ii) indicate the non-specific interaction between the CCNB surface and the fluoride ion whereas the pathway (iii) describes the specific CCNB-F interaction via ion exchange. The pH dependent adsorption behavior together with the adsorption dependent solution pH values (Fig. 4) clearly indicates a pH increase after fluoride adsorption in the acidic region (<pH 3). This favors the specific CCNB-F interaction (iii), i.e. the ligand exchange or the chemical interaction rather than non-specific or the physical interaction. However, in order to find out the contribution of non-specific CCNB-F interaction, at least partially, a detail kinetic study and energy parameter is needed and will be taken up in future communication. The decrease in fluoride uptake at higher pH can be thought to be due to the competition between hydroxyl and fluoride ions for the adsorption sites.

$$\text{Cell—Ce—OH} + \text{H}^+ + \text{F}^- \Leftrightarrow \text{Cell—Ce—F} + \text{H}_2\text{O} \quad \text{(i)}$$

$$\text{Cell—Ce—OH} + \text{H}^+ + \text{F}^- \Leftrightarrow \text{Cell—Ce—OH}_2{}^+ \cdots\cdots \text{F}^- \quad \text{(ii)}$$

$$\text{Cell—Ce—OH} + \text{F}^- \Leftrightarrow \text{Cell—Ce—F} + \text{OH}^- \quad \text{(iii)}$$

4. Conclusion

Taguchi design tool has been employed to optimize the adsorption condition of fluoride on CCNB considering the simultaneous influence of all operational variables such as pH, concentration, adsorbent dose, contact time and temperature, each at four different levels. The orthogonal array with L_{16} (4^5) layout, following the 'larger-is-better' category quality characteristics of S/N ratio was selected. This indicates that only 16 experiments are sufficient for design of the experiment. The prominent operational variables are found to be pH, concentration, adsorbent dose and temperature where pH has the highest contribution and time the least. The validity of the design and quality of predicted response was scrutinized from ANOVA. The confirmation test at the desired confidence interval quite satisfies the design. Moreover, the experimental and predicted response matches with each other. The isotherm analysis was performed with Langmuir, Freundlich and Temkin model. The quality of data fit with higher R^2 and lower SE suggests the applicability of Temkin isotherm. The fluoride interaction on CCNB may be assisted via release of hydroxyl ions. Desorption experiment with NaOH (0.01 M) showed that the CCNB can be used for three cycles, without compromising the adsorption capacity.

Acknowledgements

One of the authors (D.S) is thankful to University of Kalyani for providing a research fellowship. The authors sincerely acknowledge the support received under the UGC-SAP, DST-FIST and DST-PURSE programs.

References

Abi-aad, E., Bechara, R., Grimblot, J., & Aboukais, A. (1993). Preparation and characterization of CeO_2 under an oxidizing atmosphere. Thermal analysis XPS and EPR Study. *Chemistry of Materials*, *5*, 793–797.

Alagumuthu, G., & Ranjan, M. (2010). Kinetic and equilibrium studies on fluoride removal by zirconium (IV) impregnated ground nut shell carbon. *Hemijska Industrija*, *64*, 295–304.

Al Duri, B., & Mckay, G. (1988). Basic dye adsorption on carbon using a solid-phase diffusion model. *Chemical Engineering Journal*, *38*, 23–31.

Allen, S. J., Mckay, G., & Porter, J. F. (2004). Adsorption isotherm models for basic dye adsorption by peat in single and binary component systems. *Journal of Colloid and Interface Science*, *280*, 322–333.

Atil, H., & Unver, Y. (2000). A different approach of experimental design: Taguchi method. *Pakistan Journal of Biological Science*, *3*, 1538–1540.

Binnemans, K. (2006). Applications of tetravalent cerium compounds. In K. A. Gschneidner, J. C. G. Bunzli Jr., & V. K. Pecharsky (Eds.), *Handbook on the physics and chemistry of rare earths* (vol. 36). Elsevier. http://dx.doi.org/10.1016/S0168-1273(06)36003-5

Box, G. E. P. (1988). Signal-to-noise ratios performance criteria and transformation. *Technometrics*, *30*, 1–17.

Camacho, L. M., Torres, A., Saha, D., & Deng, S. (2010). Adsorption equilibrium and kinetics of fluoride on sol–gel-derived activated alumina adsorbents. *Journal of Colloid and Interface Science*, *349*, 307–313.

Chang, M. F., & Liu, J. C. (2007). Precipitation removal of fluoride from semiconductor wastewater. *Journal of Environmental Engineering*, *133*, 419–425.

Davila-Rodriguez, J. L., Escobar-Barrios, V. A., Shirai, K., & Rangel-Mendez, J. R. (2009). Synthesis of a chitin-based biocomposite for water treatment: Optimization for fluoride removal. *Journal of Fluorine Chemistry*, *130*, 718–726.

Deng, H., & Yu, X. (2012). Adsorption of fluoride, arsenate and phosphate in aqueous solution by cerium impregnated fibrous protein. *Chemical Engineering Journal*, *184*, 205–212.

Drouiche, N., Ghaffour, N., Lounici, H., Mameri, N., Maallemi, A., & Mahmoudi, H. (2008). Electrochemical treatment of chemical mechanical polishing wastewater: Removal of fluoride—Sludge characteristics—Operating cost. *Desalination*, *223*, 134–142.

Fang, L., Ghimire, K. N., Kuriyama, M., Inoue, K., & Makino, K. (2003). Removal of fluoride using some lanthanum(III)-loaded adsorbents with different functional groups and polymer matrices. *Journal of Chemical Technology and Biotechnology*, *78*, 1038–1047.

Fischer, R. A. (1925). *Statistical methods for research workers*. London: Oliver & Boyd.

Hench, L. L., & West, J. K. (1990). The sol–gel process. *Chemical Review*, *90*, 33–72.

Ho, Y. S., Huang, C. T., & Huang, H. W. (2002). Equilibrium sorption isotherm for metal ions on tree fern. *Process Biochemistry*, *37*, 1421–1430.

Hu, C. Y., Lo, S. L., & Kuan, W. H. (2005). Effects of the molar ratio of hydroxide and fluoride to Al(III) on fluoride removal by coagulation and electro coagulation. *Journal of Colloid and Interface Science*, *283*, 472–476.

Jagtap, S., Thakre, D., Wanjari, S., Kamble, S., Labhsetwar, N., & Rayalu, S. (2009). New modified chitosan-based adsorbent for defluoridation of water. *Journal of Colloid and Interface Science*, *332*, 280–290.

Jagtap, S., Yenkie, M. K., Labhsetwar, N., & Rayalu, S. (2012). Fluoride in drinking water and defluoridation of water. *Chemical Review*, *112*, 2454–2466.

Jayapriya, G., Ramya, R., Rathinam, X. R., & Sudha, P. N. (2011). Equilibrium and kinetic studies of fluoride adsorption by chitin/cellulose composite. *Archives of Applied Science Research*, *3*, 415–423.
Kamble, S. P., Jagtap, S., Labhsetwar, N. K., Thakare, D., Godfrey, S., Devotta, S., et al. (2007). Defluoridation of drinking water using chitin, chitosan and lanthanum-modified chitosan. *Chemical Engineering Journal*, *129*, 173–180.
Li, Z., Deng, S., Zhang, X., Zhou, W., Huang, J., & Yu, G. (2010). Removal of fluoride from water using titanium-based adsorbents. *Frontiers of Environmental Science and Engineering in China*, *4*, 414–420.
Luo, F., & Inoue, K. (2004). The removal of fluoride ion by using metal (III)-loaded amberlite resins. *Solvent Extraction and Ion Exchange*, *22*, 305–322.
Medellin-Castillo, N. A., Leyva-Ramos, R., Ocampo-Perez, R., Garcia de la Cruz, R. F., Aragon-Pina, A., Martinez-Rosales, J. M., et al. (2007). Adsorption of fluoride from water solution on bone char. *Industrial and Engineering Chemistry Research*, *46*, 9205–9212.
Meenakshi, & Maheshwari, R. C. (2006). Fluoride in drinking water and its removal. *Journal of Hazardous Materials*, *B137*, 456–463.
Meenakshi, S., & Viswanathan, N. (2007). Identification of selective ion-exchange resin for fluoride sorption. *Journal of Colloid and Interface Science*, *308*, 438–450.
Mohan, S. V., Ramanaiah, S. V., Rajkumar, B., & Sarma, P. N. (2007). Biosorption of fluoride from aqueous phase onto algal Spirogyra IO1 and evaluation of adsorption kinetics. *Bioresource Technology*, *5*, 1006–1011.
Nakamoto, K. (1978). *Infrared and Raman spectra of inorganic and coordination compounds* (3rd ed.). New York: John Wiley.
Ramos, R. (1999). Adsorption of fluoride from aqueous solution on aluminum impregnated carbon. *Carbon*, *37*, 609–617.
Rao, C. R. N., & Karthikeyan, J. (2012). Removal of fluoride from water by adsorption onto lanthanum oxide. *Water, Air, and Soil Pollution*, *223*, 1101–1114.
Rocha, R. A., & Muccillo, E. N. S. (2003). Physical and chemical properties of nano-sized powders of gadolinia-doped ceria prepared by the cation complexation technique. *Materials Research Bulletin*, *38*, 1979–1986.
Ross, P. J. (1995). *Taguchi techniques for quality engineering* (2nd ed.). New York: McGraw-Hill.
Sarkar, M., Banerjee, A., Pramanik, P. P., & Sarkar, A. R. (2006). Use of laterite for the removal of fluoride from contaminated drinking water. *Journal of Colloid and Interface Science*, *302*, 432–441.
Sarkar, M., Manna, S., & Pramanik, P. P. (2008). Evaluation of the efficiency of fly ash from thermal power plant in controlling aquatic pollution. *Journal of Indian Chemical Society*, *85*, 1130–1133.
Sehn, P. (2008). Fluoride removal with extra low energy reverse osmosis membranes: Three years of large scale field experience in Finland. *Desalination*, *223*, 73–84.
Seifi, L., Torabian, A., Kazemian, H., Bidhendi, G. N., Azimi, A. A., Nazmara, S., et al. (2011). Adsorption of BTEX on surfactant modified granulated natural zeolite nanoparticles: Parameters optimizing by applying Taguchi experimental design method. *Clean – Soil Air Water*, *39*, 939–948.
Sivasankar, V., Murugesh, S., Rajkumar, S., & Darchen, A. (2013). Cerium dispersed in carbon (CeDC) and its adsorption behavior: A first example of tailored adsorbent for fluoride removal from drinking water. *Chemical Engineering Journal*, *214*, 45–54.
Soleimani, M. T., & Kaghazchi. (2008). Adsorption of gold ions from industrial wastewater using activated carbon derived from hard shell of apricot stones – An agricultural waste. *Bioresource Technology*, *99*, 5374–5383.
Srivastava, V. C., Mall, I. D., & Mishra, I. M. (2007). Multicomponent adsorption study of metal ions onto bagasse fly ash using Taguchi's design of experimental methodology. *Industrial and Engineering Chemistry Research*, *46*, 5697–5706.
Sujana, M. G., Soma, G., Vasumathi, N., & Anand, S. (2009). Studies on fluoride adsorption capacities of amorphous Fe/Al mixed hydroxides from aqueous solutions. *Journal of Fluorine Chemistry*, *130*, 749–754.
Swain, S. K., Padhi, T., Patnaik, T., Patel, R. K., Jha, U., & Dey, R. K. (2010). Kinetics and thermodynamics of fluoride removal using cerium-impregnated chitosan. *Desalination and Water Treatment*, *13*, 369–381.
Tang, Y., Guan, X., Su, T., Gao, N., & Wang, J. (2009). Fluoride adsorption onto activated alumina: Modeling the effects of pH and some competing ions. *Colloids and Surfaces A: Physicochemical Engineering Aspects*, *337*, 33–38.
Teutli-Sequeira, A., Solache-Ríos, M., & Balderas-Hernández, P. (2012). Modification effects of hematite with aluminum hydroxide on the removal of fluoride ions from water. *Water, Air, and Soil Pollution*, *223*, 319–327.
Turner, B. D., Binning, P., & Stipp, S. L. S. (2005). Fluoride removal by calcite: Evidence for fluorite precipitation and surface adsorption. *Environmental Science and Technology*, *24*, 9561–9568.
Viswanathan, N., & Meenakshi, S. (2008). Selective sorption of fluoride using Fe(III) loaded carboxylated chitosan beads. *Journal of Fluorine Chemistry*, *129*, 503–509.
Viswanathan, N., Sundaram, C. S., & Meenakshi, S. (2009). Removal of fluoride from aqueous solution using protonated chitosan beads. *Journal of Hazardous Materials*, *161*, 423–430.
Viswanathan, G., Jaswanth, A., Gopalakrishnan, S., & Siva ilango, S. (2009). Mapping of fluoride endemic areas and assessment of fluoride exposure. *Science of the Total Environment*, *407*, 1579–1587.
Wang, D. M., Hao, G., Shi, Q. H., & Sun, Y. (2007). Fabrication and characterization of superporous cellulose bead for high-speed protein chromatography. *Journal of Chromatography A*, *1146*, 32–40.
WHO. (2008). (3rd ed.). *Guidelines for drinking-water quality* (vol. 1) Geneva: Recommendations.
Wasay, S. A., Haron, J., & Tokunaga, S. (1996). Adsorption of fluoride, phosphate, and arsenate ions on lanthanum impregnated silica gel. *Water Environment Research*, *68*, 295–300.
Xiuru, Y., Kuanxiu, S., Jianping, W., Liuchang, H., & Zhaohui, Y. (1998). Preparation of CeO_2–TiO_2/SiO_2 and its removal properties for fluoride ion. *Journal of Rare Earths*, *16*, 275–280.
Yiamouyiannis, J. (1983). *Fluoride: The aging factor*. Delaware, OH: Health Action Press.
Zhao, Y., Li, X., Liu, L., & Chen, F. (2008). Fluoride removal by Fe(III)-loaded ligand exchange cotton cellulose adsorbent from drinking water. *Carbohydrate Polymer*, *72*, 144–150.
Zhou, Y. M., Yu, C. X., & Shan, Y. (2004). Adsorption of fluoride from aqueous solution on La^{3+}-impregnated cross-linked gelatin. *Separation and Purification Technology*, *36*, 89–94.
Zolfaghari, G., Esmaili-Sari, A., Anbia, M., Younesi, H., Amirmahmoodi, S., & Ghafari-Nazari, A. (2011). Taguchi optimization approach for Pb(II) and Hg(II) removal from aqueous solutions using modified mesoporous carbon. *Journal of Hazardous Materials*, *192*, 1046–1055.